SCIENCE CHINA
Information Sciences

• RESEARCH PAPER •

April 2017, Vol. 60 042402:1–042402:11
doi: 10.1007/s11432-015-0931-8

An electrical-coupling-suppressing MEMS gyroscope with feed-forward coupling compensation and scalable fuzzy control

Chunhua HE[1,2], Jimeng ZHANG[1], Qiancheng ZHAO[1*], Qinwen HUANG[2], Zhenchuan YANG[1], Dacheng ZHANG[1] & Guizhen YAN[1]

[1]*National Key Laboratory of Science and Technology on Micro/Nano Fabrication, Institute of Microelectronics, Beijing* 100871*, China;*
[2]*Science and Technology on Reliability Physics and Application of Electronic Component Laboratory, No.*5 *Electronics Research Institute of the Ministry of Industry and Information Technology, Guangzhou* 510610*, China*

Received June 29, 2016; accepted August 24, 2016; published online January 10, 2017

Abstract This paper proposes a novel electrical coupling suppressing and drive closed loop control method for a MEMS gyroscope with feed-forward coupling compensation (FCC) and scalable fuzzy control. Theoretical analysis of the novel method is described in detail, and it is very simple to realize. Experimental results demonstrate that the electrical anti-resonant peaks located at the amplitude-frequency and phase-frequency responses are both eliminated by FCC control, and the height of the amplitude resonant peak increases more than 24 dB over 1800 Hz span. In addition, the overshoot of the transient response with scalable fuzzy control is smaller than 5%, and the settling time is less than 15 ms. The stabilities of the resonant amplitude and phase of the drive-mode velocity with scalable fuzzy control are about 15 ppm and 11 ppm, respectively. The scale factor of the gyroscope is measured to be 33.98 mV/deg/s with nonlinearity about 0.08%. Furthermore, the bias instability of the gyroscope with wavelet analysis is improved to be about 6.3 deg/h from 25.2 deg/h of the gyroscope without wavelet analysis.

Keywords MEMS gyroscope, electrical coupling suppressing, anti-resonance, feed-forward coupling compensation, scalable fuzzy control

Citation He C H, Zhang J M, Zhao Q C, et al. An electrical-coupling-suppressing MEMS gyroscope with feed-forward coupling compensation and scalable fuzzy control. Sci China Inf Sci, 2017, 60(4): 042402, doi: 10.1007/s11432-015-0931-8

1 Introduction

Electrical coupling is one of the major error sources for a MEMS gyroscope, which will deteriorate the angular rate resolution and induce the non-ideal anti-resonance to the drive and sense modes [1–3]. It is mainly attributed to the direct coupling from the excitation signal of the drive mode to the sense output through parasitic capacitances formed by the adjacent drive and sense combs [4, 5]. Thus, in order to advance the performance, it is very significant to suppress the electrical coupling signals. There

* Corresponding author (email: zqc@pku.edu.cn)

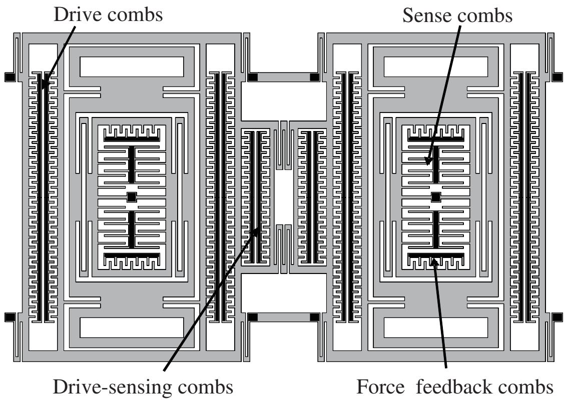

Figure 1 The simplified schematic of a Z-axis doubly decoupled MEMS tuning fork gyroscope.

are several methods to fulfill it. Symmetry design in structure and circuit benefits the cancel of electrical coupling signals when differential detection scheme is adopted simultaneously. However, the imperfection resulted from process fabrication is inevitable, so it cannot solve the issue absolutely. An isolated silicon island connected to the ground can be applied to eliminate the coupling from drive combs to the sense combs [6], but it is at the cost of extra areas.

Electromechanical amplitude modulation (EAM) [7,8] method can modulate the actual vibration signal by exerting a high-frequency carrier (usually several MHz) to the moveable mass. Thus, it can separate the effective sense signal from coupling signals. However, it needs a demodulation process to restore the useful information, which adds the complexity of the readout circuit. Moreover, it requests that the circuit could handle the demodulation in several MHz, which will increase the hardware cost, power consumption and high frequency noise. Ascending frequency drive (AFD) method [9,10] can be also used to suppress the electrical coupling by introducing a drive modulation process. Compared with EAM, it can simplify the readout circuit since it needs no extra demodulation process, but it adds complexity of the driving circuit. Similarly, it requests that the circuit could handle the modulation in high frequency domain, which will increase the cost, power consumption and noise. Hence, a simple electrical coupling suppressing method is very necessary.

On the other hand, in order to obtain stable resonant amplitude and phase of the drive-mode velocity, PID controller is widely utilized for the closed loop control [10–13]. Whereas, the control system of the drive mode is a nonlinear system, which means classical control theory is no longer suitable for the tuning of PID parameters. Although period averaging method and Routh-Hurwitz criterion [10] can be applied to judge and obtain the stability conditions, it cannot guarantee a superior control performance. Despite the transient response can be improved by adopting a 2-DOF PID controller [10], it is still not the best. Nevertheless, fuzzy algorithm is one of the most important intelligent control approaches, which can be competent for any nonlinear system control. Owing to the control rapidity and strong robustness resulted from expert experience, it can be widely used in some gyroscope control systems, such as displacement control [14], angular rate estimation [15], and automatic mode-matching control [16]. Due to a series of merits, it can be also adopted to accomplish the closed loop control for the drive mode. Therefore, this paper will present a novel and simple electrical coupling suppressing and drive closed loop control method for a MEMS gyroscope with feed forward coupling compensation (FCC) and scalable fuzzy control.

2 Theory analysis

2.1 Electrical coupling analysis

The simplified schematic of a Z-axis doubly decoupled MEMS vibratory tuning fork gyroscope is shown in Figure 1. The slide-film drive combs and slide-film drive-sensing combs are used for closed loop control of the drive mode while the squeeze-film sense combs and slide-film force feedback combs are designed for

Table 1 Key parameters of the tested gyroscope at room temperature

Parameter	Value
Sense mode capacitance	8.5 pF
Sense mode capacitance gradient	2.1 μF/m
Drive mode resonant frequency	8035.11 Hz
Drive mode quality factor	1285
Sense mode resonant frequency	7533.81 Hz
Sense mode quality factor	620

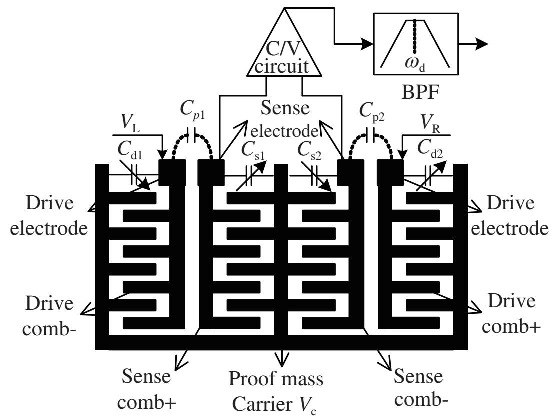

Figure 2 Electrical coupling analysis between the drive combs and sense combs of a MEMS tuning fork gyroscope.

the closed loop control of the sense mode. The gyroscope is fabricated based on SOG process and DRIE technique, which are depicted in detail in our previous work [17, 18].

The key parameters of the tested gyroscope at room temperature are listed in Table 1. Figure 2 shows that there are some parasitic capacitances between the drive combs and sense combs since they are close to each other in the structure layout, which is the major coupling source.

In Figure 2, in order to fulfill the differential detection, a DC carrier signal V_c is exerted to the proof mass. C_{d1} and C_{d2} are the differential drive capacitances, while C_{s1} and C_{s2} are the differential sense capacitances. C_{p1} and C_{p2} stand for the differential parasitic capacitances between the drive combs and sense combs. V_L and V_R represent the two differential drive signals. Owing to the existence of parasitic capacitances, drive signals can be coupled to the sense combs, which will disturb the original detection signals and deteriorate the closed loop system's stability and performance.

2.2 Novel control system

Figure 3 illustrates a block diagram of the closed loop control system for the drive mode of a MEMS gyroscope with feed-forward coupling compensation and scalable fuzzy control. It mainly comprises an analog circuit and a digital circuit. The FCC module and the coupling module are connected with solid line and dashed line, respectively. C_p is the total parasitic capacitance from the drive combs to the sense combs, while C_{pc} is a compensation capacitance applied to suppress the electrical coupling. k_{pc} is a tunable gain for FCC. Coordinated rotation digital computer (Cordic) algorithm is employed to generate the sine signals for drive and demodulation, and least mean square (LMS) algorithm is used for the sense signal demodulation, and they have been detailedly described in our previous work [19, 20]. In order to make a robust and precise control, scalable fuzzy controller, rather than PID controller, is adopted for amplitude and phase control for drive-mode velocity. From Figure 3, the original transfer function $G_d(s)$ of the controlled plant from D/A converter to A/D converter can be deducted as

$$G_d(s) = \frac{k_{cv}k_{vf}k_{dc}/m_d}{s^2 + s\omega_d/Q_d + \omega_d^2}, \tag{1}$$

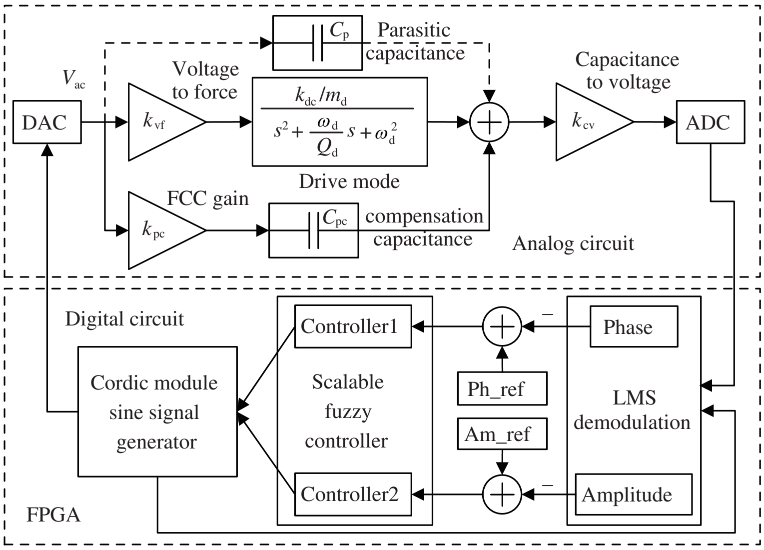

Figure 3 Block diagram of the closed loop control system for the drive mode of a MEMS gyroscope with feed-forward coupling compensation (FCC) and scalable fuzzy control.

where $\omega_{\rm d}$ and $Q_{\rm d}$ are the resonant frequency and quality factor of the drive mode, respectively. $k_{\rm vf}$, $k_{\rm dc}$ and $k_{\rm cv}$ are the gains of voltage to force module, displacement to capacitance module, and capacitance to voltage module, respectively. $m_{\rm d}$ stands for the drive mass. ${\rm Re}(G_{\rm d})$ and ${\rm Im}(G_{\rm d})$ are the real and imaginary parts of $G_{\rm d}(s)$, as shown in (2) and (3),

$$
{\rm Re}(G_{\rm d}) = \frac{(\omega_{\rm d}^2-\omega^2)k_{\rm cv}k_{\rm vf}k_{\rm dc}/m_{\rm d}}{(\omega_{\rm d}^2-\omega^2)^2+\omega^2\omega_{\rm d}^2/Q_{\rm d}^2}, \tag{2}
$$

$$
{\rm Im}(G_{\rm d}) = \frac{-\omega\omega_{\rm d}k_{\rm cv}k_{\rm vf}k_{\rm dc}/(m_{\rm d}Q_{\rm d})}{(\omega_{\rm d}^2-\omega^2)^2+\omega^2\omega_{\rm d}^2/Q_{\rm d}^2}. \tag{3}
$$

However, take into account the electrical coupling, the controlled plant $G_{\rm dc}(s)$ can be derived as

$$
G_{\rm dc}(s) = \frac{k_{\rm cv}C_{\rm p}[s^2+s\omega_{\rm d}/Q_{\rm d}+(\omega_{\rm d}^2+k_{\rm vf}k_{\rm dc}/m_{\rm d}C_{\rm p})]}{s^2+s\omega_{\rm d}/Q_{\rm d}+\omega_{\rm d}^2}. \tag{4}
$$

Due to the existence of electrical coupling, the controlled plant is changed to be a notch filter, and the characteristics of frequency response will be deteriorated. ${\rm Re}(G_{\rm dc})$ and ${\rm Im}(G_{\rm dc})$ are the real and imaginary parts of $G_{\rm dc}(s)$, as shown in (5) and (6),

$$
{\rm Re}(G_{\rm dc}) = \frac{(\omega_{\rm d}^2-\omega^2)k_{\rm cv}k_{\rm vf}k_{\rm dc}/m_{\rm d}}{(\omega_{\rm d}^2-\omega^2)^2+\omega^2\omega_{\rm d}^2/Q_{\rm d}^2}+k_{\rm cv}C_{\rm p}, \tag{5}
$$

$$
{\rm Im}(G_{\rm dc}) = \frac{-\omega\omega_{\rm d}k_{\rm cv}k_{\rm vf}k_{\rm dc}/(m_{\rm d}Q_{\rm d})}{(\omega_{\rm d}^2-\omega^2)^2+\omega^2\omega_{\rm d}^2/Q_{\rm d}^2}. \tag{6}
$$

Compared with (2) and (3), we can see that the imaginary parts of $G_{\rm d}(s)$ and $G_{\rm dc}(s)$ are the same, but the real parts of them are different. The difference of the two real parts is $k_{\rm cv}C_{\rm p}$, and the larger are $k_{\rm cv}$ and $C_{\rm p}$, the bigger is the difference.

From (4), there is an anti-resonant peak located at the amplitude-frequency response, whose resonant frequency $\omega_{\rm dc}$ and quality factor $Q_{\rm dc}$ are yielded as

$$
\omega_{\rm dc} = \sqrt{\omega_{\rm d}^2+k_{\rm vf}k_{\rm dc}/m_{\rm d}C_{\rm p}}, \tag{7}
$$

$$
Q_{\rm dc} = \frac{Q_{\rm d}}{\omega_{\rm d}}\sqrt{\omega_{\rm d}^2+k_{\rm vf}k_{\rm dc}/m_{\rm d}C_{\rm p}}. \tag{8}
$$

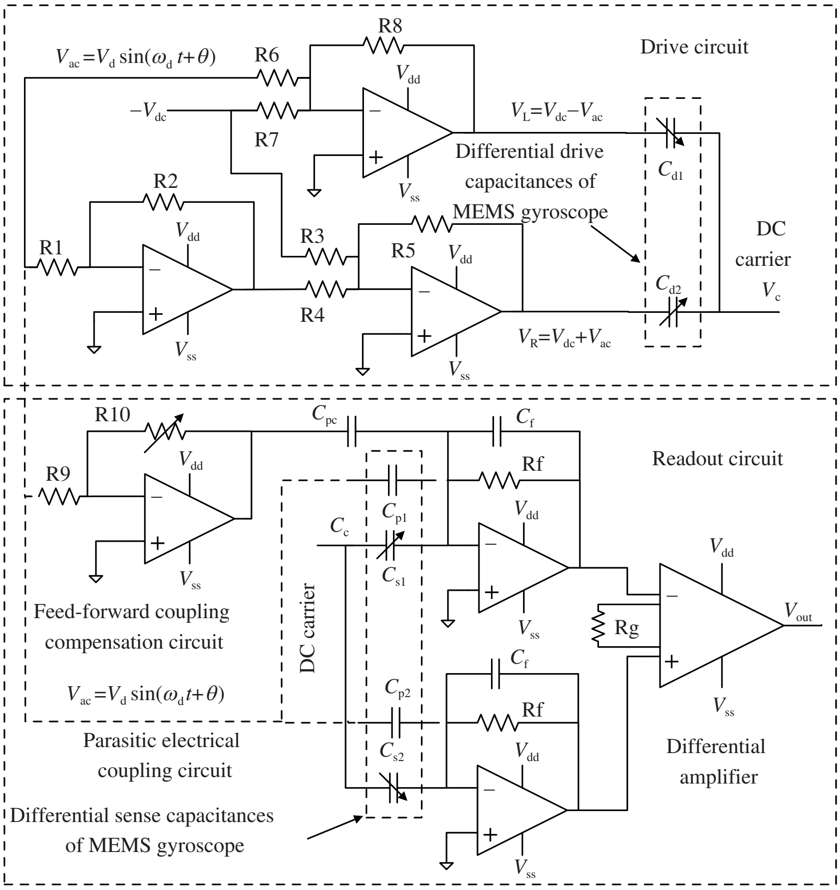

Figure 4 The schematic of the differential drive and readout circuits with feed-forward coupling compensation control.

The difference between $\omega_{\rm dc}$ and $\omega_{\rm d}$ is determined by $k_{\rm vf}k_{\rm dc}/m_{\rm d}C_{\rm p}$, as well as the difference between $Q_{\rm dc}$ and $Q_{\rm d}$. When FCC is added to the control loop and Eq. (9) is satisfied, the controlled plant shown in (4) can be converted back to (1), which means the anti-resonance effect is eliminated absolutely.

The schematic of the differential drive and readout circuits with FCC control is depicted in Figure 4. FCC circuit and the coupling circuit are connected with solid line and dashed line, respectively. Charge amplifier or trans-impedance amplifier is applied to detect the displacement or velocity signal. $V_{\rm dc}$ and $V_{\rm ac}$ are the DC and AC signals exerted to the drive combs, respectively. Carrier $V_{\rm c}$ is a DC signal, and there is no drive modulation and carrier demodulation in the control loop, which vastly decreases the hardware cost, power consumption and high frequency noise compared with those methods mentioned above. Furthermore, FCC circuit only comprises an inverter and a compensation capacitance, which is very simple and easy to realize. $k_{\rm pc}$ and $C_{\rm pc}$ are set according to $C_{\rm p}$, and $C_{\rm p}$ can be measured by coupling swept frequency test in advance when $V_{\rm c}$ is connected to the ground. Thus, based on the parameters set in the readout circuit and the amplitude-frequency response, $C_{\rm p}$ can be finally evaluated,

$$C_{\rm p} = -k_{\rm pc}C_{\rm pc}. \tag{9}$$

2.3 Scalable fuzzy controller

Since fuzzy controller is competent for any nonlinear system control, it is employed for the closed loop control of the drive mode in this work, as shown in Figure 3. The formula of the traditional incremental two-dimensional fuzzy controller can be described as [16]

$$V_n = V_{n-1} + \Delta V_n = V_{n-1} + {\rm fuzzy}(k_{\rm p}E, k_{\rm d}{\rm EC}), \tag{10}$$

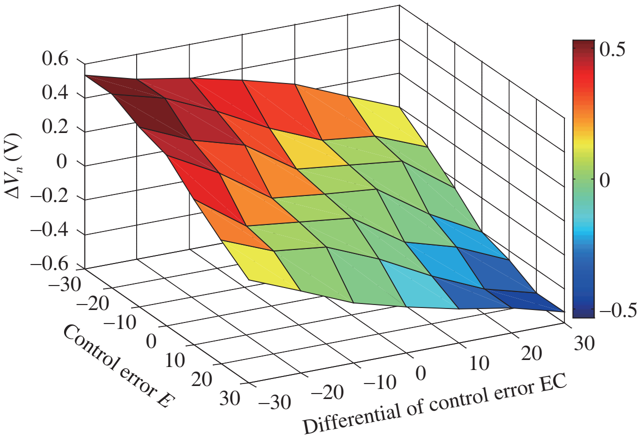

Figure 5 The output increment of the fuzzy controller ΔV_n varies with the control error E and the differential of the control error EC.

where V_n and V_{n-1} are the current and the last output, and ΔV_n is the output increment determined by the fuzzy controller. k_p and k_d are the weights of the control error E and the differential of the control error EC, respectively. E, EC and ΔV_n consist of seven language values {nb, nm, ns, ze, ps, pm, pb} on the discourse of $[-3, 3]$. nb, nm, ns, ze, ps, pm, pb represent negative big, negative medium, negative small, zero, positive small, positive medium and positive big, respectively. The rule table is the core of a fuzzy controller, which is set based on expert experience. The 49 fuzzy rules are established according to the following principles: (a) If E and EC are large, ΔV_n should be adjusted to reduce the error rapidly. (b) If E and EC are small, ΔV_n should be tuned to suppress overshoot and eliminate static error.

According to the fuzzy rules and Mamdani algorithm, a look-up table (LUT) for fuzzy control can be calculated with the following formula:

$$\Delta V_n' = \bigcup_{i=1}^{49} (E' \text{ and } \mathrm{EC}') \circ [(E_i \text{ and } \mathrm{EC}_i) \rightarrow \Delta V_{ni}], \tag{11}$$

where E' and EC' are the typical inputs of E and EC; E_i, EC_i and ΔV_{ni} are the fuzzy rules for determining the mapping relationship of fuzzy sets. Afterwards, centroid method is used for defuzzification of $\Delta V_n'$ to obtain ΔV_n. Finally, the control LUT can be stored in the memory of FPGA chip to save computing time and resources. The relationship between E, EC and ΔV_n is depicted in Figure 5. It shows that ΔV_n varies with E and EC sensitively.

The traditional fuzzy controller is similar to a nonlinear PD controller, as shown in (10), which results in a non-ideal control precision due to the finite 49 fuzzy rules, 7 quantized steps and lack of an integration component. Therefore, traditional fuzzy algorithm should be improved to enhance the control precision. Here, a scale factor α is introduced to tune the quantized step size and control increment, as depicted in

$$V_n = V_{n-1} + \Delta V_n = V_{n-1} + \alpha \cdot \mathrm{fuzzy}(\alpha k_\mathrm{p} E, \alpha k_\mathrm{d} \mathrm{EC}). \tag{12}$$

In order to further minimize E and EC, α is often set to be 2^k (k is an integer), which can enhance the control speed and precision. The core concepts of the scalable fuzzy algorithm are based on the following rules: (a) If E and EC are judged as ze, the quantized step size and control increment should be shrunk to advance control precision, and α is minified by half. (b) If E and EC is judged as pb or nb, the quantized step size and control increment should be amplified to enhance control speed, and α is magnified twice. (c) Otherwise, α is not changed. The initial value of α is set to be 1 (k=0).

Thus, the scalable fuzzy controller can achieve a rapid and accurate control for any nonlinear or uncertain system with finite fuzzy rules and quantized steps, and it is simpler to realize than a 2-DOF PID controller.

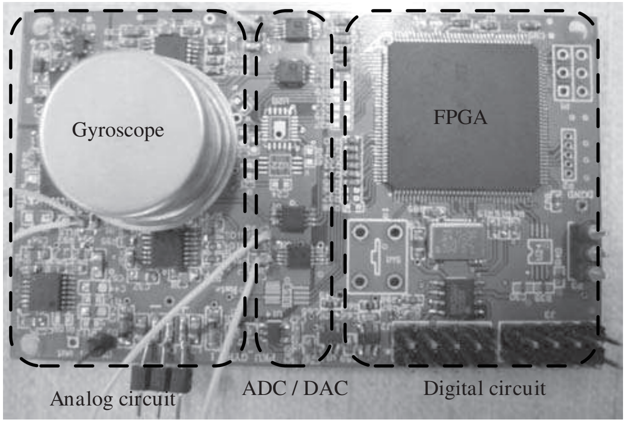

Figure 6 The mixed signal circuit for a vacuum packaging gyroscope.

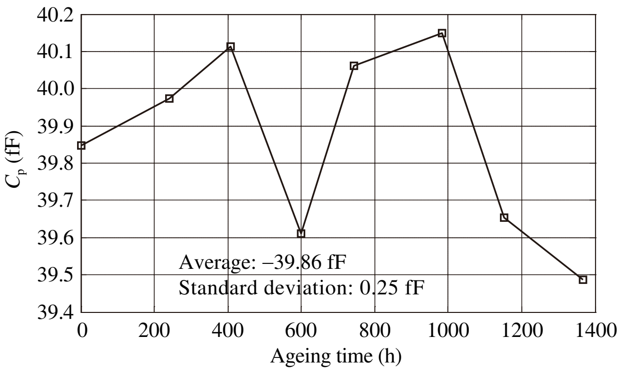

Figure 7 The relationship between the total parasitic capacitance C_{p} and the ageing time.

3 Experimental results

3.1 Electrical coupling suppressing

The mixed signal circuit for a vacuum packaging gyroscope is illustrated in Figure 6. It mainly includes an analog circuit and a digital circuit. FCC is realized in the analog circuit and scalable fuzzy control is accomplished in the digital circuit with FPGA device.

As described above, C_{p} can be measured by coupling swept frequency test in advance when V_{c} is connected to the ground. Then, based on the parameters set in the readout circuit and the amplitude-frequency response, C_{p} can be finally evaluated, as shown in Figure 7. In order to obtain the long-term stability of C_{p}, an accelerated test is conducted with a high temperature chamber, whose temperature is set to be 125°C according to the standard GJB548B-2005 1015.1. C_{p} is measured at the ageing time of [0 240 408 600 744 984 1152 1368] h. Figure 7 figures out that the average is 39.86 fF and standard deviation is 0.25 fF, which means C_{p} is stable enough and changes less with time.

Experimental results indicate that the electrical anti-resonant peaks are located at the amplitude-frequency and phase-frequency responses when there is no FCC control, which seriously deteriorates the original response characteristics, as shown in Figure 8. However, they are both eliminated when a simple FCC circuit is adopted. The height of the amplitude resonant peak increases more than 24 dB over 1800 Hz span, and the phase characteristic is also improved by 180 deg, which verifies the novel method is effective. Closed loop control for the drive mode aims to make the gyroscope resonant and obtain the stable amplitude of the drive velocity. From (4), the electrical coupling signal cannot change the resonant frequency of the peak, however, it will affect the amplitude and phase of the peak. Hence, it should be eliminated for enhancing the control performance. The improvement of phase characteristic proves the electrical coupling signal is suppressed and benefits the stability of the closed loop control system.

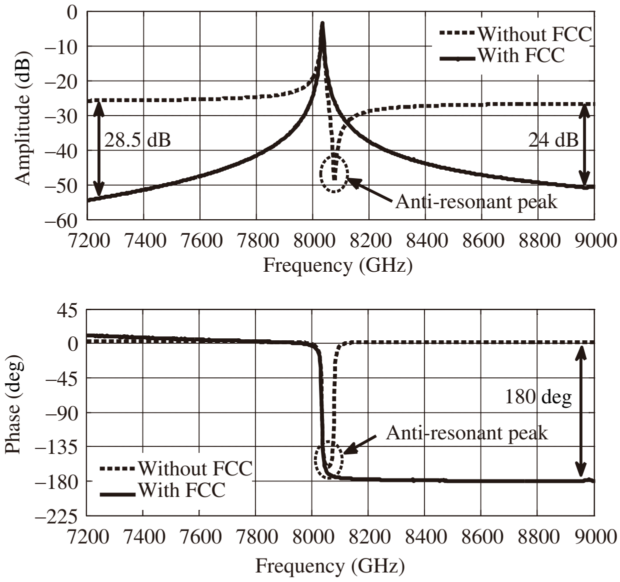

Figure 8 The frequency responses of the drive mode with and without feed-forward coupling compensation (FCC).

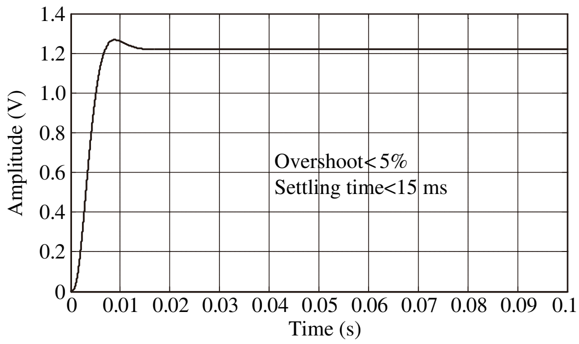

Figure 9 Transient response of the amplitude of the drive-mode velocity with scalable fuzzy control.

3.2 Closed loop control for the drive mode

The transient response of the amplitude of the drive-mode velocity with scalable fuzzy control is shown in Figure 9. It figures out that the overshoot is smaller than 5% and the settling time is less than 15 ms, which validates the closed loop system with scalable fuzzy control is robust and the control speed is so rapid. Compared with the control effects reported in [10], scalable fuzzy control is superior to 2-DOF PID control as for a nonlinear system.

The average of the resonant amplitude of the dive-mode velocity of the MEMS gyroscope with scalable fuzzy control is 1222.29 mV with standard deviation about 18.78 μV, while the average of the resonant phase is −89.827 deg with standard deviation about 0.983 mdeg. Thereby, the stabilities of them are evaluated to be about 15 ppm and 11 ppm, respectively, as depicted in Figures 10 and 11, which indicates the novel control system is stable and effective.

3.3 Performance tests

Figure 12 demonstrates that the scale factor and nonlinearity of the gyroscope with FCC and scalable fuzzy control are measured to be 33.98 mV/deg/s and 0.08%, respectively. Wavelet analysis algorithm has been proved effective to suppress the high-frequency noise in some work [21, 22], thus it is also employed here. The bias instability of the gyroscope with wavelet analysis is improved to be about 6.3 deg/h from 25.2 deg/h of the gyroscope without wavelet analysis, as shown in Figure 13.

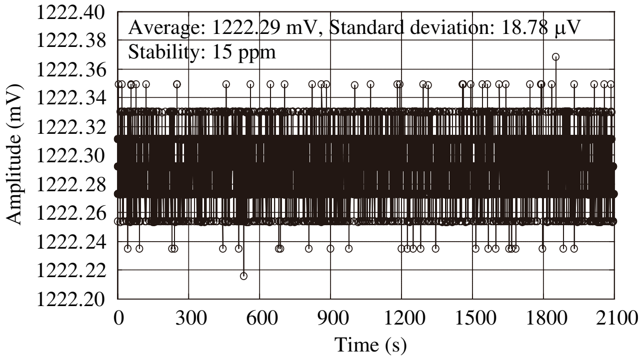

Figure 10 Stability test of the amplitude of the drive-mode velocity with scalable fuzzy control.

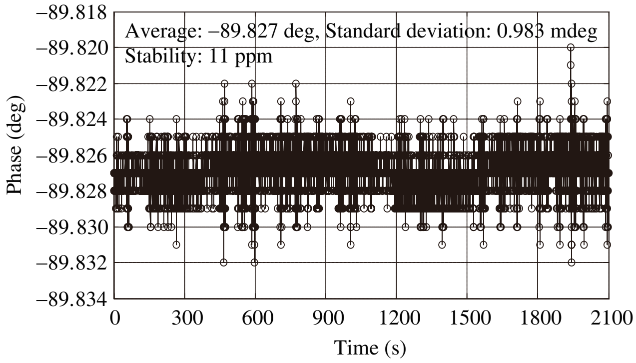

Figure 11 Stability test of the phase of the drive-mode velocity with scalable fuzzy control.

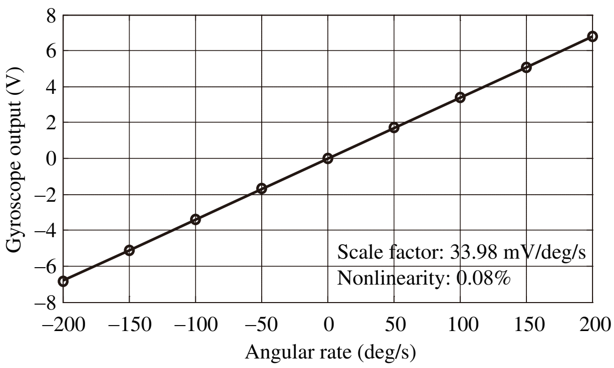

Figure 12 Scale factor test of the MEMS gyroscope with feed-forward coupling compensation and scalable fuzzy control.

4 Conclusion

This paper has presented a novel electrical coupling suppressing and drive closed loop control method for a MEMS gyroscope with (FCC) feed-forward coupling compensation and scalable fuzzy control. Theoretical analysis of the novel method is described in detail, and it is very simple to realize. Experimental results demonstrate that the electrical anti-resonant peaks located at the amplitude-frequency and phase-frequency responses are both eliminated by FCC control, and the height of the amplitude resonant peak increases more than 24 dB over 1800 Hz span. In addition, the overshoot of the transient response with scalable fuzzy control is smaller than 5%, and the settling time is less than 15 ms. The stabilities of the resonant amplitude and phase of the drive-mode velocity with scalable fuzzy control are about 15 ppm and 11 ppm, respectively. The scale factor of the gyroscope is measured to be 33.98 mV/deg/s with nonlinearity about 0.08%. Moreover, the bias instability of the gyroscope with wavelet analysis is improved to be about 6.3 deg/h from 25.2 deg/h of the gyroscope without wavelet analysis. Therefore,

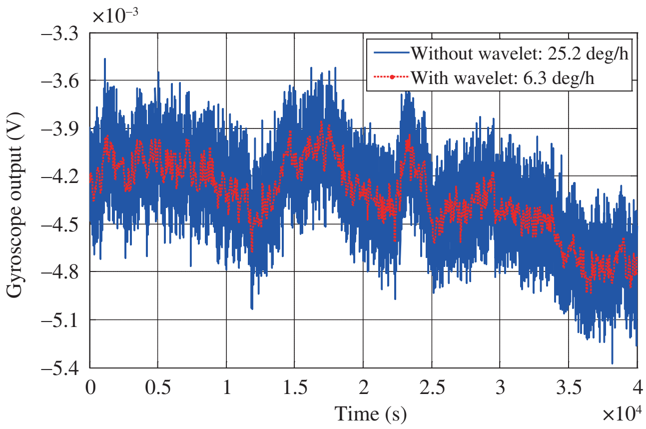

Figure 13 Bias drift tests of the MEMS gyroscope with and without wavelet analysis processing.

the proposed FCC and scalable fuzzy control method is feasible and effective, and it can be also applied to other fields.

Acknowledgements This work was partially supported by National Natural Science Foundation of China (Grant Nos. 61434003, 51505089).

Conflict of interest The authors declare that they have no conflict of interest.

References

1 Lee A, Ko H, Cho D I D, et al. Non-ideal behavior of a driving resonator loop in a vibratory capacitive microgyroscope. Microelectronics J, 2008, 39: 1–6
2 Acar C, Shkel A M. An approach for increasing drive-mode bandwidth of MEMS vibratory gyroscopes. J Microelectromech Syst, 2005, 14: 520–528
3 Alper S E, Akin T. A symmetric surface micro-machined gyroscope with decoupled oscillation modes. Sensors Actuat A Phys, 2002, 97–98: 347–358
4 Weinberg M S, Kourepenis A. Error sources in in-plane silicon tuning-fork MEMS gyroscopes. J Microelectromech Syst, 2006, 15: 479–491
5 Saukoski M, Aaltonen L, Halonen K A I, et al. Zero-rate output and quadrature compensation in vibratory MEMS gyroscopes. IEEE Sensors J, 2007, 7: 1639–1652
6 Guo Z Y, Liu X S, Yang Z C, et al. Electrostatic isolation structure for linearity improvement of a lateral-axis tuning fork gyroscope. In: Proceedings of IEEE 23rd International Conference on Micro Electro Mechanical Systems (MEMS), Hong Kong, 2010. 264–267
7 Cagdaser B, Jog A, Last M, et al. Capacitive sense feedback control for MEMS beam steering mirrors. In: Proceedings of Solid-State Sensor and Actuator Workshop, Hilton Head Island, 2004. 348–351
8 Acar C, Shkel A M. Structurally decoupled micromachined gyroscopes with post-release capacitance enhancement. J Micromech Microeng, 2005, 15: 1092–1101
9 Cui J, Guo Z Y, Yang Z C, et al. Electrical coupling suppressing for a microgyroscope using ascending frequency drive with 2-DOF PID controller. In: Proceedings of the 16th International Solid-State Sensors, Actuators and Microsystems Conference (TRANSDUCERS), Beijing, 2011. 2002–2005
10 Cui J, Guo Z Y, Yang Z C, et al. Electrical coupling suppression and transient response improvement for a microgyroscope using ascending frequency drive with a 2-DOF PID controller. J Micromech Microeng, 2011, 21: 095020
11 Trusov A A, Prikhodko I P, Rozelle D M, et al. 1 PPM precision self calibration of scale factor in MEMS Coriolis vibratory gyroscopes. In: Proceedings of Transducers & Eurosensors XXVII: the 17th International Conference on Solid-State Sensors, Actuators and Microsystems (TRANSDUCERS & EUROSENSORS XXVII), Barcelona, 2013. 2531–2534
12 Woo J K, Cho J Y, Boyd C, et al. Whole-angle-mode micromachined fused-silica birdbath resonator gyroscope (WA-BRG). In: Proceedings of the 27th IEEE International Conference on Micro Electro Mechanical Systems (MEMS), San Francisco, 2014. 20–23
13 Senkal D, Ng E J, Hong V, et al. Parametric drive of a toroidal MEMS rate integrating gyroscope demonstrating <20 ppm scale factor stability. In: Proceedings of the 28th IEEE International Conference on Micro Electro Mechanical Systems (MEMS), Estoril, 2015. 29–32
14 Xiao Q J, Li S Y, Chen W Y, et al. Fuzzy tuning PI control for initial levitation of micromachined electrostatically levitated gyroscope. Electron Lett, 2009, 45: 818–819

15 Fei J T, Xin M Y. An adaptive fuzzy sliding mode controller for MEMS triaxial gyroscope with angular velocity estimation. Nonlinear Dyn, 2012, 70: 97–109

16 He C H, Zhao Q C, Huang Q W, et al. A MEMS vibratory gyroscope with real-time mode-matching and robust control for the sense mode. IEEE Sensors J, 2015, 15: 2069–2077

17 Ding H T, Yang Z C, Zhang M L, et al. Experimental study on the footing effect for SOG structures using DRIE. J Semicond, 2008, 29: 1088–1093

18 Ding H T, Liu X S, Lin L T, et al. A High-resolution silicon-on-glass axis gyroscope operating at atmospheric pressure. IEEE Sensors J, 2010, 10: 1066–1074

19 Liu Y X, He C H, Liu D C, et al. Digital closed-loop driver design of micromechanical gyroscopes based on coordinated rotation digital computer algorithm. In: Proceedings of the 8th IEEE International Conference on Nano/Micro Engineered and Molecular Systems (NEMS), Suzhou, 2013. 1145–1148

20 Liu D C, He C H, Zhao Q C, et al. Digital signal processing for a micromachined vibratory gyroscope based on a three dimensional adaptive filter demodulator. Measurement, 2014, 50: 198–202

21 Li Z P, Fan Q J, Chang L M, et al. Improved wavelet threshold denoising method for MEMS gyroscope. In: Proceedings of the 11th IEEE International Conference on Control & Automation (ICCA), Taichung, 2014. 530–534

22 Stebler Y, Guerrier S, Skaloud J, et al. Generalized method of wavelet moments for inertial navigation filter design. IEEE Trans Aerospace Electron Syst, 2014, 50: 2269–2283